http://communications.science.ankara.edu.tr

Commun.Fac.Sci.Univ.Ank.Ser. A1 Math. Stat.
Volume 72, Number 2, Pages 530–550 (2023)
DOI:10.31801/cfsuasmas.1087827
ISSN 1303-5991 E-ISSN 2618-6470

Research Article; Received: March 14, 2022; Accepted: November 22, 2022

FHD FLOW IN AN IRREGULAR CAVITY SUBJECTED TO A NON-UNIFORM MAGNETIC FIELD

Pelin ŞENEL
Department of Mathematics, Karadeniz Technical University, Trabzon, TÜRKİYE

Abstract. In this paper FHD flow in a rectangular pipe constricted by two analogous semi-cylinders attached to the left and the bottom walls is investigated. The laminar, axial flow is produced by a constant pressure gradient, and the flow is affected by a spatially varying non-uniform magnetic field caused by two electric wires. The current-carrying wires are placed along the axes of the semi-cylinders. The fully developed flow is studied on the 2D cross-section of the pipe, a cavity, where the wires act as point magnetic sources. The pressure equation is added to the mathematical model, and the velocity-pressure form governing equations are numerically solved by the dual reciprocity boundary element method (DRBEM). The Dirichlet type pressure boundary conditions are approximated through a process using the radial basis functions and a finite difference. The flow, velocity, and pressure variations are investigated for different magnetic field strengths and current ratios. The grid independence study is also carried out. The proposed iterative scheme is capable of generating numerical results by performing a non-uniform discretization for the boundary. Dense discretizations are applied at the places where the flow shows a sudden fluctuation. It is shown by the numerical results that the flow and the pressure variations are dominated by the strong magnetic source. With an increment in the magnetic number, the planar flow is accelerated, the axial flow is decelerated, and the pressure increases, especially around the strong point magnetic source.

1. Introduction

The interaction of electromagnetic fields and the fluid mechanics may be grouped into three main categories, namely electrohydrodynamics (EHD), magnetohydrodynamics (MHD), and ferrohydrodynamics (FHD) [27]. Electrohydrodynamics theory investigates the flow of electrically charged particles under the influence of electric

2020 *Mathematics Subject Classification.* 65N38, 76D05, 76W05.
Keywords. FHD flow, variable magnetic field, DRBEM, pressure computation.
psenel@ktu.edu.tr; 0000-0002-2096-7521

fields. In EHD, the electrostatic force term plays a crucial role in the momentum equations. EHD phenomena is used in designs of many engineering instruments such as pumps, printing systems, flow meters, etc. The motion of electrically conducting fluids in the presence of magnetic fields is the subject of magnetohydrodynamics. In MHD, the body force acting on the fluid is called Lorentz force. Lorentz force retards the core flow and accelerates the side flows, thus equalizes the total flow in pipes. Ferrohydrodynamics is an interdisciplinary subject having an inherent interest of a physical and mathematical nature with applications in printing [7], medicine [44], tribiology [14], separation science [47], cooling systems [32], microelectromechanical systems (MEMS) [48], etc. FHD investigates the motion of electrically insulated (non-conducting) fluid under the effect of magnetic polarization [27]. In FHD, there needs no presence of electric current flow in the fluid, but the flow undergoes a fluctuation due to the material magnetization. A ferrofluid is mainly composed of a carrier fluid (e.g. water) and nanoscale magnetic particles (e.g iron, nickel) coated by a surfactant. Biomagnetic fluid dynamics is also based on the FHD phenomena. Blood is the mostly known biomagnetic fluid which possesses its magnetization property by the hemoglobin molecule.

The spatially varying non-uniform magnetic field generated by the current-carrying wires applies a volumetric force to the fluid and has been used to control the flow in pipes. The volumetric force, so-called the Kelvin force density, drives the magnetic particles, and the translational and rotational motion of these particles are transferred to the ferrofluid. The resulting body forces alter the flow in pipes. Therefore in applications where the flow regulation is substantial the ferrofluid is a preferential choice [6].

Much computational research has been carried out on the FHD flows in pipes due to their vast variety of applications. The FHD flows in pipes are modeled in terms of the continuity and the Navier-Stokes equations. If there is heat transfer, then the energy equation is added to the system. The governing equations are coupled with highly nonlinear partial differential equations (PDEs) containing diffusion, convection, and force terms. Therefore, approximate solutions are required to understand the flow and the pressure behaviors. The pressure-linked pseudo transient method (PLEM), finite difference method (FDM), finite volume method (FVM), and finite element method (FEM) are mostly used numerical approaches to tackle the FHD flows.

The PLEM was used to investigate the effect of a single current-carrying wire placed below the rectangular pipe in [42]. It was reported that the solutions show an oscillatory behavior on a common-grid. A mathematical model on the same flow configuration for the electrically conducting fluid was presented in [41]. In that paper, both uniform and non-uniform magnetic field effects on the biomagnetic fluid flow were studied. It was concluded that the form of the magnetic field gradient substantially determines the flow in the pipe. Mousavi et al. [23] used a commercial software based on the finite volume methodology to investigate the

biomagnetic flow in a three-dimensional pipe under the influence of a magnetic field due to a single current-carrying wire. They obtained grid-independent results by using a discretization covering the magnetic field accurately. The influence of an alternating magnetic field that is generated by line source dipoles on a forced convective ferrofluid flow was investigated by Goharkhah and Ashjaee [10] using a control volume technique. They reported the flow acceleration along the surface as the ferrofluid passes over the magnetic field section. Recently, A finite volume approach for a nanofluid flow through an annular pipe subjected to multiple magnetic sources was presented by Soltanipour [40]. A control volume-based FEM solution of a free convection ferrofluid flow in an enclosure subjected to multiple current-carrying wires was presented in [37]. Loukopoulos and Tzirtzilakis [19] presented a FDM solution of a biomagnetic fluid flow between two horizontal plates subjected to a single current-carrying wire. Some other computational studies on magnetizable fluids can be found in [1, 3, 15, 22, 25, 28, 29, 33–36, 38, 39].

The boundary elements method (BEM) [4] is an alternative to domain discretization type methods such as FDM and FEM. In BEM, fundamental solutions are required to transform the partial differential equations into boundary integral equations. After the insertion of the boundary conditions, a shuffling process is applied to collect all the unknowns on one side of the equation. The resultant dense nonsymmetric linear equation is then treated by using an appropriate direct or iterative solver. The boundary-only discretization advantage of the BEM reduces computational time and memory usage. When the partial differential equation is nonlinear, containing body forces or time dependence, the corresponding BEM integral equation includes domain integrals. DRBEM has arisen to tackle this difficulty. In DRBEM [24], a simpler equation's fundamental solution is employed and the remaining terms are treated through a series expansion using radial basis functions, and then the reciprocity procedures are applied. The DRBEM has been applied to many types of physical problems from elasticity to fluid dynamics. Some recent advances in the DRBEM applications may be found in [2, 11, 16, 21, 31, 45, 46].

The previous studies demonstrated that no consideration has been given to pressure computations for FHD irregular cavity flows. Most of the present studies used domain-type numerical methods which are computationally expensive. The novelty of the present study is that low computational cost solutions for the velocity and the pressure of FHD flow in an irregular domain are presented. Therefore, the flow of a ferrofluid through a pipe subjected to a non-uniform magnetic field that is generated by two variable electric wires is investigated. The effects of the magnetic field strength and the current ratio variations are discussed. The pressure profiles are presented for the first time in the literature. The current-carrying wires are placed parallel to one of the horizontal and the vertical walls. The geometry of the pipe is formed in such a way that the current-carrying wires do not touch the electrically insulated walls. The fully developed flow is modeled on the two dimensional

cross-section of the pipe that is taken vertical to the axial flow. The governing equations in primitive variables (velocity-pressure form) are discretized by the DRBEM, and an iterative numerical solution procedure is suggested. It is observed that a non-uniform discretization is required to capture the flow behaviors. The flow and pressure variations are dominated by the electric wire possessing high current intensity. The proposed numerical scheme is capable of generating grid-independent solutions for the velocity and the pressure with less computational cost. This is the first DRBEM study on the FHD flow in a pipe contracted by two semi-cylinders carrying variable electric currents along their axes. The proposed numerical scheme provides the pressure variation which is very important in engineering design. This study is an extension of a presentation that is published as an abstract [30] at the International Conference on Applied Mathematics in Engineering (ICAME'21).
The rest of the paper is organized in the following fashion. In Section 2, the physics of the problem is introduced, and the construction of the mathematical model is presented. The numerical solution procedure and the pressure boundary condition approximations are explained in Section 3. In Section 4, the numerical solutions and discussions are presented. The consequences achieved from the present study are collected in Section 5.

2. Physical Problem and Mathematical Model

A laminar, steady, fully developed flow of an electrically insulated, magnetizable fluid is considered in a long rectangular pipe. Two semi-cylinders with radiuses $\bar{r}$ are located in the middle of the left and the bottom walls. Two electric wires (W_1 and W_2) are passing through the axes of the semi-cylinders. The pipe walls are electrically insulated. The 3D flow configuration is presented in Figure 1.

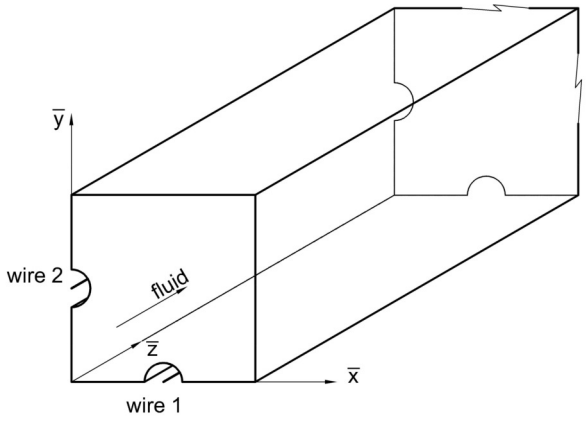

Figure 1. Fully developed flow in a pipe

The flow is driven by a constant pressure gradient in the $\bar{z}-$direction, and it is under the influence of a non-uniform magnetic field that is generated by the two wires carrying electric currents with different intensities (I_1 and I_2). The fully developed flow is modeled on the 2D cross-section of the pipe. On this cross-section (cavity), wires behave alike as point magnetic sources. Each section of the cavity boundary is smooth. Figure 2 displays the 2D problem geometry.

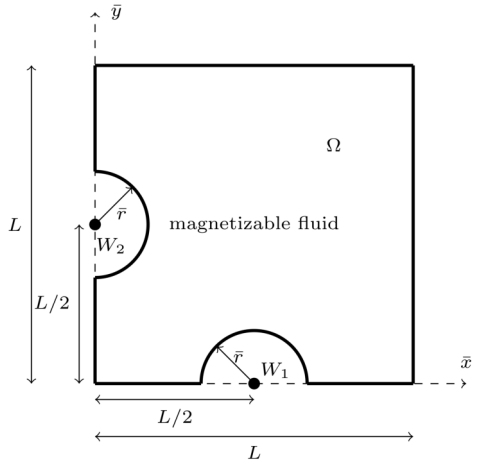

FIGURE 2. Problem geometry

The FHD flow in a cavity is defined by the continuity and Navier-Stokes equations containing the dimensional velocity $\bar{\mathbf{V}}(\bar{x},\bar{y}) = (\bar{u}(\bar{x},\bar{y}),\bar{v}(\bar{x},\bar{y}),\bar{w}(\bar{x},\bar{y}))$ and the pressure $\bar{P}(\bar{x},\bar{y},\bar{z})$ [27]. Once the flow reaches a fully developed state, the velocity and the pressure of the fluid do not vary in the pipe axis direction.

$$\frac{\partial \bar{u}}{\partial \bar{x}} + \frac{\partial \bar{v}}{\partial \bar{y}} = 0, \tag{1}$$

$$\bar{u}\frac{\partial \bar{u}}{\partial \bar{x}} + \bar{v}\frac{\partial \bar{u}}{\partial \bar{y}} = -\frac{1}{\rho}\frac{\partial \bar{P}}{\partial \bar{x}} + \nu\left(\frac{\partial^2 \bar{u}}{\partial \bar{x}^2} + \frac{\partial^2 \bar{u}}{\partial \bar{y}^2}\right) + \frac{\mu_0 \bar{M}}{\rho}\frac{\partial \bar{H}}{\partial \bar{x}}, \tag{2}$$

$$\bar{u}\frac{\partial \bar{v}}{\partial \bar{x}} + \bar{v}\frac{\partial \bar{v}}{\partial \bar{y}} = -\frac{1}{\rho}\frac{\partial \bar{P}}{\partial \bar{y}} + \nu\left(\frac{\partial^2 \bar{v}}{\partial \bar{x}^2} + \frac{\partial^2 \bar{v}}{\partial \bar{y}^2}\right) + \frac{\mu_0 \bar{M}}{\rho}\frac{\partial \bar{H}}{\partial \bar{y}}, \tag{3}$$

$$\bar{u}\frac{\partial \bar{w}}{\partial \bar{x}} + \bar{v}\frac{\partial \bar{w}}{\partial \bar{y}} = -\frac{1}{\rho}\frac{\partial \bar{P}}{\partial \bar{z}} + \nu\left(\frac{\partial^2 \bar{w}}{\partial \bar{x}^2} + \frac{\partial^2 \bar{w}}{\partial \bar{y}^2}\right), \tag{4}$$

where ρ and ν are the density and the kinematic viscosity of the fluid, μ_0 is the magnetic permeability of vacuum, and $\bar{H}$ is the magnetic field intensity. $\bar{M} = \chi\bar{H}$ is the magnetization where χ is the magnetic susceptibility of the fluid. Since the fluid is electrically insulated the force terms on the right-hand side of the momentum

equations are containing only the magnetization force in FHD. This mathematical model does not have an analytical solution.
In fully developed flows pressure $\bar{P}$ can be written as [9]

$$\bar{P}(\bar{x},\bar{y},\bar{z}) = \bar{P}_1(\bar{z}) + \bar{p}(\bar{x},\bar{y}). \tag{5}$$

Since the axial flow is generated by a constant pressure gradient, one has

$$\frac{\partial \bar{P}}{\partial \bar{z}} = \frac{\partial \bar{P}_1}{\partial \bar{z}} = \bar{P}_z = \text{constant} \ . \tag{6}$$

The components of the magnetic field $\bar{\mathbf{H}} = (\bar{H}_x(\bar{x},\bar{y}), \bar{H}_y(\bar{x},\bar{y}), 0)$ generated by infinitely long, thin wires carrying steady electric currents I_1 and I_2 flowing in the same direction are given by [17, 26]

$$\bar{H}_x = -\frac{1}{2\pi}\sum_{i=1}^{2} \frac{I_i(\bar{y}-\bar{b}_i)}{(\bar{x}-\bar{a}_i)^2+(\bar{y}-\bar{b}_i)^2}, \qquad \bar{H}_y = \frac{1}{2\pi}\sum_{i=1}^{2} \frac{I_i(\bar{x}-\bar{a}_i)}{(\bar{x}-\bar{a}_i)^2+(\bar{y}-\bar{b}_i)^2}, \tag{7}$$

where $(\bar{a}_i, \bar{b}_i)$, $i = 1, 2$, are the locations of the point magnetic sources around the cavity. The point magnetic sources have different strengths. The intensity of the magnetic field generated by the two point magnetic sources is defined by

$$\bar{H} = \sqrt{\bar{H}_x^2 + \bar{H}_y^2} \ . \tag{8}$$

For the numerical simulations following non-dimensional variables are introduced

$$x = \frac{\bar{x}}{L}, \quad y = \frac{\bar{y}}{L}, \quad z = \frac{\bar{z}}{L}, \quad u = \frac{\bar{u}L}{\nu}, \quad v = \frac{\bar{v}L}{\nu}, \quad w = \frac{\bar{w}L}{\nu}, \quad P = \frac{\bar{P}L^2}{\rho\nu^2}, \quad H = \frac{\bar{H}}{H_0}. \tag{9}$$

Here, L is the height of the cavity, and $H_0 = I_1/(2\pi L)$.
The governing equations in the dimensionless form are

$$\frac{\partial u}{\partial x} + \frac{\partial v}{\partial y} = 0, \tag{10}$$

$$\frac{\partial^2 u}{\partial x^2} + \frac{\partial^2 u}{\partial y^2} = \frac{\partial p}{\partial x} + u\frac{\partial u}{\partial x} + v\frac{\partial u}{\partial y} - MnH\frac{\partial H}{\partial x}, \tag{11}$$

$$\frac{\partial^2 v}{\partial x^2} + \frac{\partial^2 v}{\partial y^2} = \frac{\partial p}{\partial y} + u\frac{\partial v}{\partial x} + v\frac{\partial v}{\partial y} - MnH\frac{\partial H}{\partial y}, \tag{12}$$

$$\frac{\partial^2 w}{\partial x^2} + \frac{\partial^2 w}{\partial y^2} = P_z + u\frac{\partial w}{\partial x} + v\frac{\partial w}{\partial y}, \tag{13}$$

where Mn is the magnetic number defined by

$$Mn = \frac{\mu_0 \chi H_0^2 L^2}{\nu^2 \rho} \ . \tag{14}$$

To investigate the pressure variation within the cavity, the equation of pressure is obtained. Eqs (11) and (12) are differentiated with respect to x and y, respectively. The resultant equations are added and some terms are canceled using the continuity equation. Then, the pressure equation is obtaied

$$\frac{\partial^2 p}{\partial x^2}+\frac{\partial^2 p}{\partial y^2} = Mn(\left(\frac{\partial H}{\partial x}\right)^2+\left(\frac{\partial H}{\partial y}\right)^2+H(\frac{\partial^2 H}{\partial x^2}+\frac{\partial^2 H}{\partial y^2}))-\left(\frac{\partial u}{\partial x}\right)^2-\left(\frac{\partial v}{\partial y}\right)^2-2\frac{\partial v}{\partial x}\frac{\partial u}{\partial y}\,. \tag{15}$$

The flow patterns in 2D cavities are visualized by the stream function Ψ isolines (streamlines). The stream function satisfies the continuity equation and is linked with the planar velocities in $x-$ and $y-$directions as

$$u = \frac{\partial \Psi}{\partial y}, \quad v = -\frac{\partial \Psi}{\partial x}. \tag{16}$$

From the continuity equation, the stream function equation is generated

$$\frac{\partial^2 \Psi}{\partial x^2} + \frac{\partial^2 \Psi}{\partial y^2} = \frac{\partial u}{\partial y} - \frac{\partial v}{\partial x}\,. \tag{17}$$

Non-dimensional forms of the magnetic field components are

$$H_x = -\frac{y-b_1}{(x-a_1)^2+(y-b_1)^2} - I_r\frac{y-b_2}{(x-a_2)^2+(y-b_2)^2}, \tag{18}$$

$$H_y = \frac{x-a_1}{(x-a_1)^2+(y-b_1)^2} + I_r\frac{x-a_2}{(x-a_2)^2+(y-b_2)^2}, \tag{19}$$

where $I_r = I_2/I_1$ is the current ratio, (a_1, b_1), (a_2, b_2) are the positions of magnetic sources and

$$H = \sqrt{H_x^2 + H_y^2}. \tag{20}$$

No-slip boundary condition is applied on the cavity walls, thus

$$u = v = w = \Psi = 0 \qquad \text{on} \;\; \partial\Omega. \tag{21}$$

Here, $\partial\Omega$ stands for the boundary of the cavity Ω. Dirichlet-type pressure boundary conditions are obtained approximately by using a finite difference scheme and the radial basis functions. The details for the pressure boundary condition computations are given in the next section.

3. Application of the DRBEM

The governing partial differential equations (11)-(13), (15), and (17) are transformed into boundary integral equations by the DRBEM. The governing equations are rewritten in the Poisson type as

$$\nabla^2 R = b_R, \tag{22}$$

where R denotes u, v, w, p, or Ψ. b_R is the right-hand side of the equation for R containing convection and force terms. For the sake of practice, the construction of the DRBEM discretized system has been presented on this sample equation.

Eq. (22) is weighted by the fundamental solution of the Laplace equation ($u^* = (1/2\pi)\ln(1/r)$, [24]) and then the Green's first identity is applied to achieve

$$c_i R_i + \int_\Gamma R q^* d\Gamma - \int_\Gamma u^* \frac{\partial R}{\partial n} d\Gamma = -\int_\Omega b_R u^* d\Omega, \tag{23}$$

with $\Gamma = \partial\Omega$ and $q^* = \partial u^*/\partial n$ notations. $c_i = \theta/2\pi$ where θ radian is the internal angle at the source point i. $c_i = 1/2$ on the smooth part of the boundary and $c_i = 1$ for the interior nodes.

b_R is approximated by using linear radial basis functions $f_j(r_i) = 1 + r_{ij}$, $(r_{ij} = \sqrt{(x_i - x_j)^2 + (y_i - y_j)^2})$ to eliminate the domain integral on the right-hand side of Eq. (23). The corresponding particular solutions $\hat{u}_j$ satisfy $\nabla^2 \hat{u}_j = f_j$. Then, by using the collocation technique one gets an approximation for b_R as

$$b_R \approx \sum_{j=1}^{N+L} (\alpha_R)_j f_j = \sum_{j=1}^{N+L} (\alpha_R)_j \nabla^2 \hat{u}_j, \tag{24}$$

where $(\alpha_R)_j$'s are the unspecified coefficients. Here, N is the number of boundary nodes and L is the number of interior nodes.

Substituting the approximation in 24 into the integral equation 23 one has Laplace term on the right-hand side of the equation (23). Green's first identity is applied again and the irregular boundary is discretized by the constant elements. Then, the corresponding boundary integral equation is obtained

$$c_i R_i + \sum_{k=1}^{N} \int_{\Gamma_k} R q^* d\Gamma - \sum_{k=1}^{N} \int_{\Gamma_k} u^* \frac{\partial R}{\partial n} d\Gamma = \sum_{j=1}^{N+L} (\alpha_R)_j \Big(c_i \hat{u}_{ij} + \sum_{k=1}^{N} \int_{\Gamma_k} \hat{u}_j q^* d\Gamma - \sum_{k=1}^{N} \int_{\Gamma_k} u^* \frac{\partial \hat{u}_j}{\partial n} d\Gamma\Big) . \tag{25}$$

Considering all of the nodes, Eq. (24) gives

$$\mathbf{b_R} = \mathbf{F}\boldsymbol{\alpha_R}. \tag{26}$$

Here, $\mathbf{b_R}$ and $\boldsymbol{\alpha_R}$ are $(N + L) \times 1$ vectors. $(N + L) \times (N + L)$ sized DRBEM coordinate matrix $\mathbf{F}$ is constructed from the radial basis functions as $\mathbf{F}_{ij} = f_{ij}$. According to Micchelli's Theorem [20], $\mathbf{F}$ is invertible.

Thus, the vector of unspecified coefficients $\boldsymbol{\alpha_R}$ is calculated from Eq. (26) as

$$\boldsymbol{\alpha_R} = \mathbf{F}^{-1}\mathbf{b_R}. \tag{27}$$

Considering all the discretization nodes and using equations (25) and (27) the system of matrix-vector equations are obtained

$$\mathbf{H}u - \mathbf{G}\frac{\partial u}{\partial n} = (\mathbf{H}\hat{\mathbf{U}} - \mathbf{G}\hat{\mathbf{Q}})\mathbf{F}^{-1}\Big(\frac{\partial p}{\partial x} + u\frac{\partial u}{\partial x} + v\frac{\partial u}{\partial y} - MnH\frac{\partial H}{\partial x}\Big), \tag{28}$$

$$\mathbf{H}v - \mathbf{G}\frac{\partial v}{\partial n} = (\mathbf{H}\hat{\mathbf{U}} - \mathbf{G}\hat{\mathbf{Q}})\mathbf{F}^{-1}\Big(\frac{\partial p}{\partial y} + u\frac{\partial v}{\partial x} + v\frac{\partial v}{\partial y} - MnH\frac{\partial H}{\partial y}\Big), \tag{29}$$

$$\mathbf{H}w - \mathbf{G}\frac{\partial w}{\partial n} = (\mathbf{H}\hat{\mathbf{U}} - \mathbf{G}\hat{\mathbf{Q}})\mathbf{F}^{-1}(P_z + u\frac{\partial w}{\partial x} + v\frac{\partial w}{\partial y}), \tag{30}$$

$$\begin{aligned}\mathbf{H}p - \mathbf{G}\frac{\partial p}{\partial n} =&(\mathbf{H}\hat{\mathbf{U}} - \mathbf{G}\hat{\mathbf{Q}})\mathbf{F}^{-1}(Mn(\left(\frac{\partial H}{\partial x}\right)^2 + \left(\frac{\partial H}{\partial y}\right)^2 + H\nabla^2 H) - \left(\frac{\partial u}{\partial x}\right)^2 \\ &- \left(\frac{\partial v}{\partial y}\right)^2 - 2\frac{\partial v}{\partial x}\frac{\partial u}{\partial y}),\end{aligned} \tag{31}$$

$$\mathbf{H}\Psi - \mathbf{G}\frac{\partial \Psi}{\partial n} = (\mathbf{H}\hat{\mathbf{U}} - \mathbf{G}\hat{\mathbf{Q}})\mathbf{F}^{-1}(\frac{\partial u}{\partial y} - \frac{\partial v}{\partial x}), \tag{32}$$

The entries of $(N+L)\times(N+L)$ sized DRBEM matrices are

$$\begin{aligned}\mathbf{H}_{ij} &= c_i\delta_{ij} + \int_{\Gamma_j} q^* d\Gamma_j, \\ \mathbf{G}_{ij} &= \int_{\Gamma_j} u^* d\Gamma_j, \qquad \mathbf{G}_{ii} = \frac{l}{2\pi}(ln(\frac{2}{l}) + 1).\end{aligned} \tag{33}$$

Here, δ_{ij} is the Kronecker delta and l is the length of the constant element. The diagonal entries of $\mathbf{G}$ are computed analytically due to the singularities of the integrals. $\hat{\mathbf{U}}_{ij} = \hat{u}_{ij}$ and $\hat{\mathbf{Q}}_{ij} = \hat{q}_{ij}$, $\hat{q}_{ij} = \partial\hat{u}_{ij}/\partial n$.
Using the advantage of DRBEM, all the space derivatives of the unknowns in Eqs. (28)-(32) are treated by using the approximation

$$\hat{\mathbf{R}} = \mathbf{F}\xi, \tag{34}$$

where $\hat{\mathbf{R}}$ represent u, v, w, or p and ξ denotes an unspecified coefficient vector. Then one has

$$\frac{\partial \hat{\mathbf{R}}}{\partial \eta} = \frac{\partial \mathbf{F}}{\partial \eta}\mathbf{F}^{-1}\hat{\mathbf{R}}, \tag{35}$$

with η being x or y.
Once all the DRBEM constructions are completed Dirichlet type boundary conditions are inserted, and all the problem unknowns are carried to the left-hand side. This process is called shuffling. Then, one obtains a full linear system $\mathbf{A}\mathbf{x} = \tilde{\mathbf{b}}$. The $(N+L)\times(N+L)$ sized coefficient matrix $\mathbf{A}$ is dense having no special form. Thus, the resultant linear system is numerically solved by the LU decomposition method with less computational cost.
An iterative solution process is applied. Initially, planar velocity components are taken as zero everywhere. As can be observed from Eqs. (11) and (12) in this case, magnetization forces are balanced by the pressure gradients [27]. The iteration process is started with $\partial p/\partial x = MnH(\partial H/\partial x) + 10^{-12}$ and $\partial p/\partial y = MnH(\partial H/\partial y) + 10^{-12}$ initial values for the pressure gradients. Firstly, planar velocity equations (Eq. (28) and (29)) are solved. To treat the nonlinear terms, unknown velocities are taken from the previous iteration level and their space derivatives are taken from the new level. Boundary conditions for the pressure

are computed repeatedly in each iteration level by using newly obtained planar velocity nodal solutions. Then, the pressure equation (Eq. (31)) is solved. Lastly, the axial velocity and the stream function equations (Eqs. (30) and (32), respectively) are solved with given boundary conditions. At each level, previously computed problem unknowns are used in the subsequent equations. Pressure is relaxed as a weighted summation of the nodal values taken from the previous and new iteration levels, $p^{(n+1)} = rp^{(n+1)} + (1-r)p^{(n)}$ where $0 < r < 1$. The stopping criterion for the iterative process is

$$\frac{||z^{(n+1)} - z^{(n)}||_\infty}{||z^{(n)}||_\infty} < 10^{-3}, \tag{36}$$

where z represents u, v, p, or Ψ and n is the number of iteration.

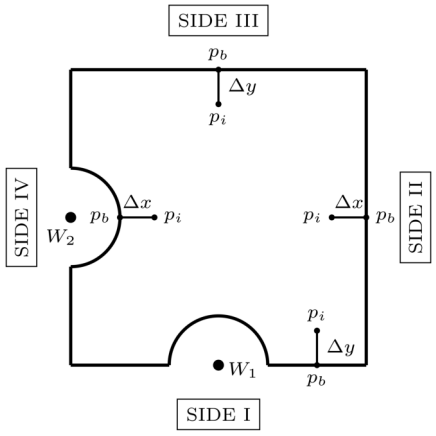

FIGURE 3. Pressure boundary condition approximation

Pressure boundary conditions are obtained by using Eqs. (11) and (12). Pressure gradients are approximated by a forward or backward difference and the terms containing the space derivatives of the planar velocities are approximated by the DRBEM coordinate matrix $\mathbf{F}$. Formulations of approximate boundary conditions for the pressure are found for each side of the cavity (Figure 3) as

$$\text{SIDE I:} \quad p_b^{(n+1)} = p_i^{(n)} - \Delta y(\mathbf{S}v^{(n+1)} + MnH\frac{\partial H}{\partial y}), \tag{37}$$

$$\text{SIDE II:} \quad p_b^{(n+1)} = p_i^{(n)} + \Delta x(\mathbf{S}u^{(n+1)} + MnH\frac{\partial H}{\partial x}), \tag{38}$$

$$\text{SIDE III:} \quad p_b^{(n+1)} = p_i^{(n)} + \Delta y(\mathbf{S}v^{(n+1)} + MnH\frac{\partial H}{\partial y}), \tag{39}$$

$$\text{SIDE IV:} \quad p_b^{(n+1)} = p_i^{(n)} - \Delta x(\mathbf{S}u^{(n+1)} + MnH\frac{\partial H}{\partial x}), \tag{40}$$

where p_i is the closest interior node to the corresponding boundary node p_b and

$$\mathbf{S} = \frac{\partial \mathbf{F}}{\partial x}F^{-1}\frac{\partial \mathbf{F}}{\partial x}F^{-1} + \frac{\partial \mathbf{F}}{\partial y}F^{-1}\frac{\partial \mathbf{F}}{\partial y}F^{-1} - \mathbf{u}^{(n+1)}\frac{\partial \mathbf{F}}{\partial x}F^{-1} - \mathbf{v}^{(n+1)}\frac{\partial \mathbf{F}}{\partial y}F^{-1}, \tag{41}$$

with $\mathbf{u}^{(n+1)}$ and $\mathbf{v}^{(n+1)}$ being the diagonal matrices constructed from $u-$ and $v-$velocity nodal solutions at the $(n+1)$st iteration, respectively.

$P_z = -8000$ is taken as in [42] and $(a_1, b_1) = (0.5, 0)$, $(a_2, b_2) = (0, 0.5)$ are the placement of point magnetic sources around the cavity. The radiuses of the semi-cylinders are $r = \bar{r}/L = 0.1$.

4. Numerical results and discussions

The influences of magnetization force and current ratio variations on the FHD cavity flow are investigated for various combinations of Mn and I_r. Numerical results are illustrated in terms of velocity, pressure, and stream function contour plots. The computer code is validated with the existing literature, a grid independence study is carried out, and an appropriate non-uniform discretization is suggested.

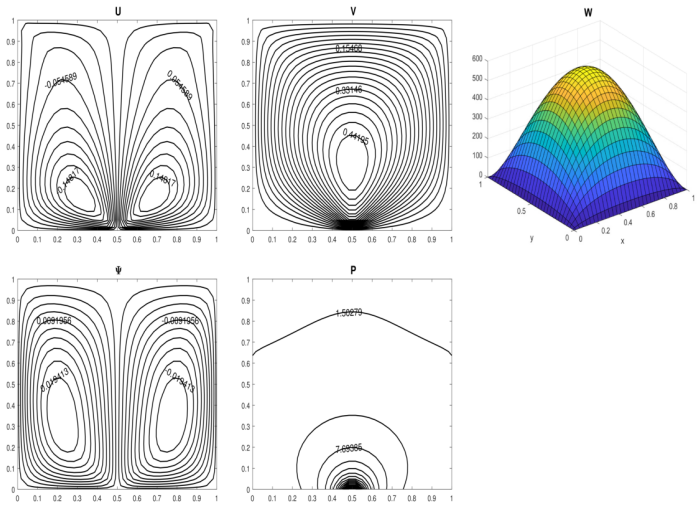

Figure 4. Square cavity flow subjected to unique point source $Mn = 90$.

The validation of the numerical procedure and the written computer code is carried out for an FHD square cavity flow subjected to a unique point source that is placed at $(0.5, -0.05)$. Figure 4 displays the flow and pressure behaviors when

$Mn = 90$. A good agreement is observed in the flow behaviors between the present study and the existing literature [42].

The magnetization force pushes the fluid towards the top wall therefore the flow on the transverse plane is separated into two symmetric vortices rotating in opposite directions. The movement of the fluid particles in front of the point magnetic source causes highly concentrated pressure at the bottom of the cavity. The $u-$velocity is divided into two vortices and the $v-$velocity is expanded through the channel section forming a boundary layer in front of the magnetic source. For small Mn values, axial velocity shows a parabolic profile.

The grid independence test is carried for $N = 192, 240, 288, 336, 384$. The numerical solutions for the pressure and the planar velocities are compared along the $x = 0.25$ line for $Mn = 10$, $I_r = 1$. Figure 5 shows that $N = 336$ gives grid-independent solutions.

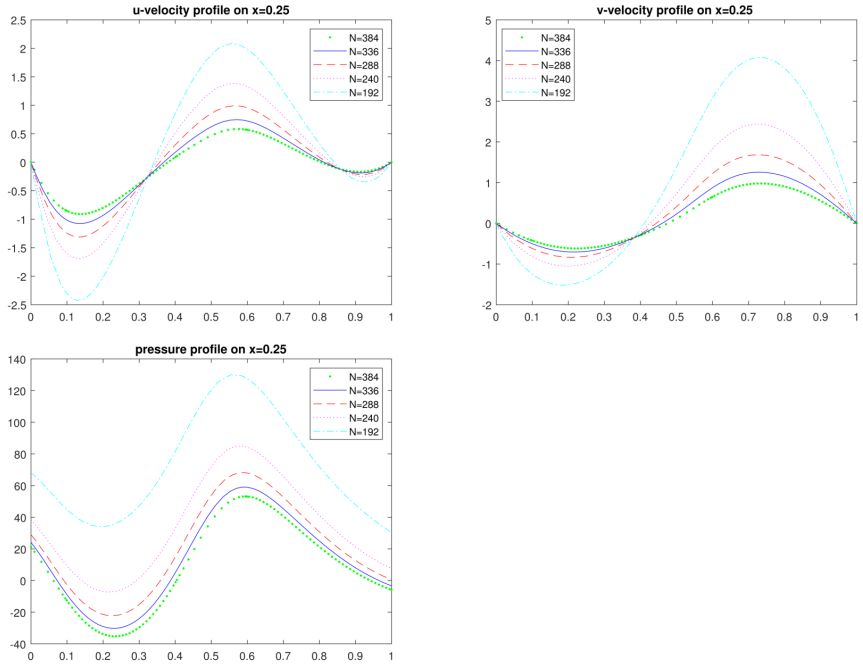

FIGURE 5. Grid independence test along the $x = 0.25$ line for $Mn = 10$, $I_r = 1$.

Table 1 displays the number of iterations needed to achieve solutions with a tolerance of 10^{-3} for $Mn = 10$, $I_r = 1$. It is observed that the number of iterations increases almost linearly as the number of boundary nodes advances. Effects of magnetic sources on the pressure and velocity behaviors are investigated for various

N=192	N=240	$N = 288$	$N = 336$	$N = 384$
573	670	812	957	1106

TABLE 1. Number of iterations for different N when $Mn = 10$, $I_r = 1$.

combinations of current ratios I_r and moderate values of magnetic numbers Mn. The boundary of the 2D computational domain is non-uniformly discretized by constant elements. In constant element discretization, the approximate solution is constant on each element and the points where the unknown values are considered (nodes) are in the middle of the element. This property enables one to deal with the corners of the irregular cavity. Each element is taken from the smooth part of the boundary section. Figure 6 shows samples for the discretization of the boundaries and the choices of the interior nodes. More interior nodes are taken at the places where the flow is expected to show a sudden fluctuation according to the strengths of the point magnetic sources and the cavity corners. In the case of the same current intensities (e.g. (a) $I_r = 1$) the discretizations are dense near the corners of the cavity. When one of the point magnetic sources is stronger than the other (e.g. (b) $I_r = 0.2$) more interior nodes are taken in front of the semi-circles.

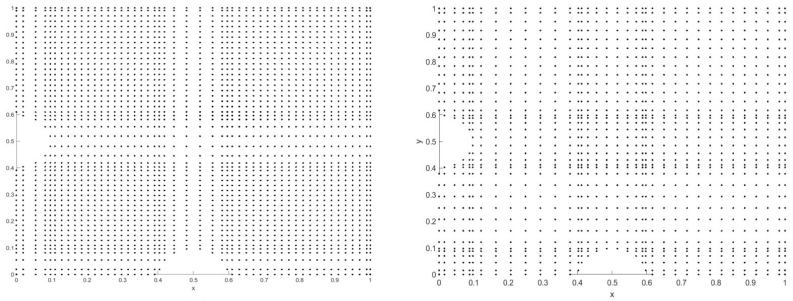

(a) (b)

FIGURE 6. Sample discretizations of the boundary and the choice of the interior nodes. (a) $I_r = 1$, (b) $I_r = 0.2$. $Mn = 10$.

The number of boundary elements is increased with Mn. At most $N = 400$ boundary and $L = 9888$ interior nodes are used for the discretization. The numerical solutions are achieved using a 64GB RAM computer.

Figure 7 shows velocity, pressure, and the stream function contour plots when both magnetic sources have the same strength ($I_r = 1$). The magnetic sources push the fluid through the opposite walls and apply the same magnetization force. This causes the division of the flow on the transverse plane into vortices that are

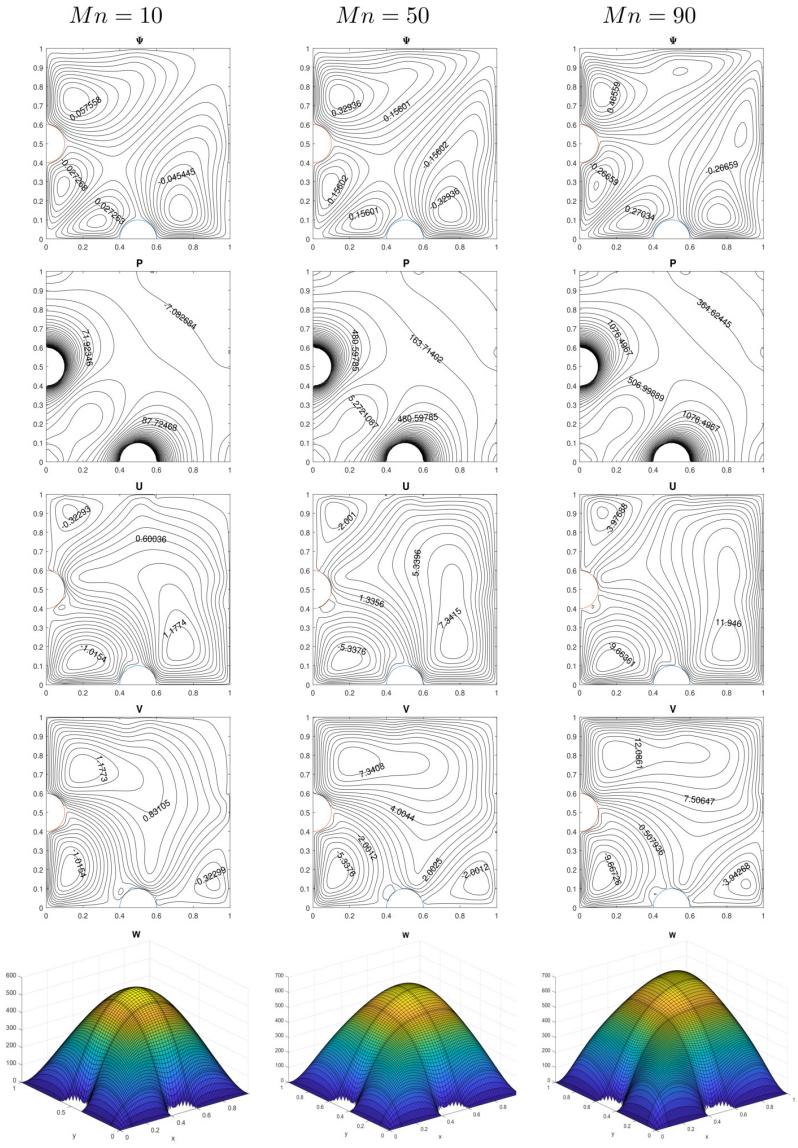

FIGURE 7. Velocity and pressure profiles for $I_r = 1$, $Mn = 10, 50, 90$.

symmetric about the $y = x$ axis, and the boundary layers are formed. Four symmetric vortices that are rotating in opposite directions are generated. Magnetic

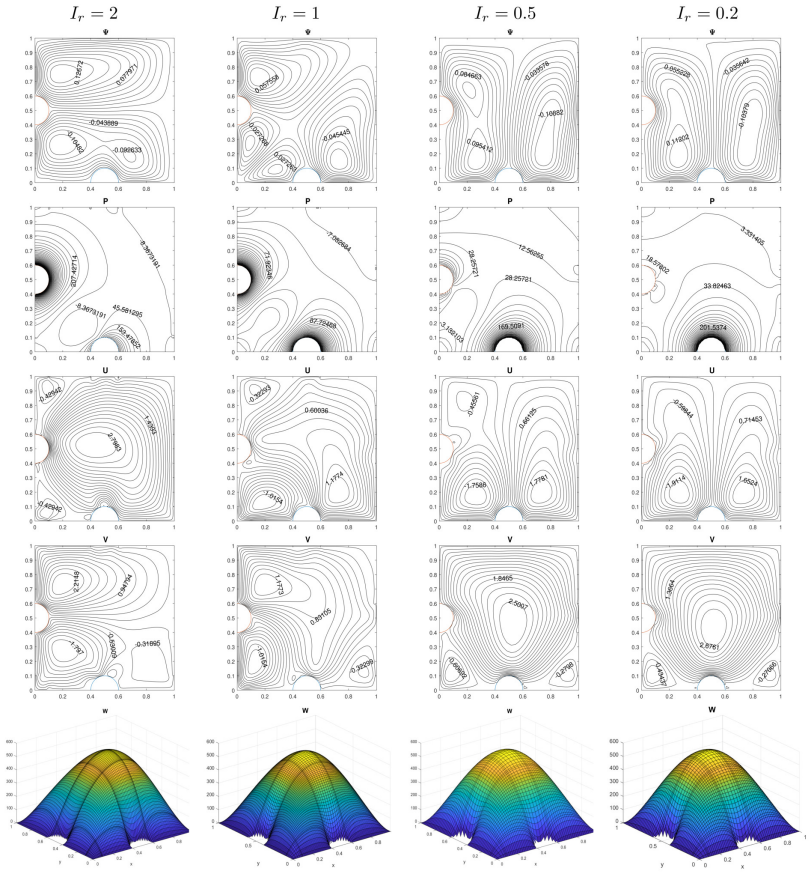

FIGURE 8. Velocity and pressure profiles for $Mn = 10$, $I_r = 0.2, 0.5, 1, 2$.

sources suppress the effects of each other, and therefore two small vortices appear at the left bottom corner of the cavity. Pressure is high around the semi-circles due to the large velocity gradients in these areas. Axial flow shows a parabolic profile obeying the shape of the cavity. $u-$ and $v-$velocity behaviors are similar due to the symmetric location of the point sources. When the ratio of the currents is kept fixed and the magnetic number increases, the magnetic field strengths of both wires increase at the same rate. Thus, an increment in Mn accelerates the planar flow (u and v velocity advance) and retards the axial flow around the semi-circles. The pressure in the cavity increases. Strong vortices are developed on the transverse plane as Mn advances. This is a well-known effect of the increment in the magnetic

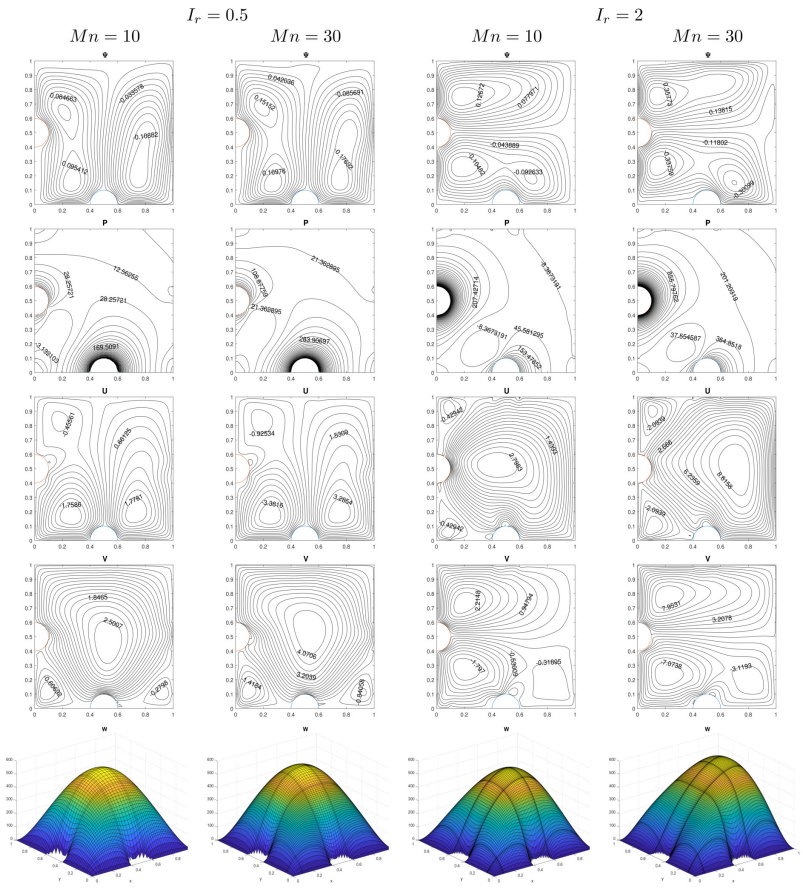

FIGURE 9. Velocity and pressure profiles for $I_r = 0.5, 2$ and $Mn = 10, 30$.

field strength.

The effect of the magnetic field generated by two wires with different current intensities is investigated for a fixed Mn. This corresponds to the case when I_1 is kept constant and I_2 changes. Figure 8 shows the flow and the pressure profiles for $I_r = I_2/I_1 = 2, 1, 0.5, 0.2$. Generally, the flow and pressure behaviors are dominated by the strong point magnetic source. When one of the point magnetic sources is two times stronger than the other one ($I_r = 0.5, 2$) two vortices develop in front of the dominant source that is analogous to the unique point source case. The weak source force the fluid to divide the vortex in front of it. Pressure concentration is high near the strong source. The flow retardation in the axial direction is mainly

observed in front of the dominant point magnetic source. Planar velocity profiles are generally dominated by the strong source, except for a little deformation caused by the weak source. When the current intensity of the point source below the cavity increases (comparing $I_r = 0.5$ and $I_r = 0.2$ cases) the magnetization force applied by the strong source is increased and the flow is dominated mainly by the strong bottom point magnetic source. The flow in the cavity nearly behaves as if there was a single-point magnetic source. Pressure around the week source decreases.

In Figure 9, the effect of the magnetic number increase is investigated when one of the sources is two times stronger than the other ($I_r = 0.5$ and $I_r = 2$ cases). An increase in Mn advances the force applied to the fluid in the cavity and accelerates the planar flow. At the same time, axial velocity decreases due to the kinetic energy transfer in the axial direction into the transverse plane. The pressure in the cavity increases, and the axial flow retardation is significant, especially near the dominant magnetic source.

5. Conclusion

In this study, FHD flow in a rectangular duct constricted by two semi-cylinders under the influence of a non-uniform magnetic field is investigated. The flow is modeled in the velocity-pressure formulation and the numerical results are obtained using the DRBEM. The Dirichlet type pressure boundary conditions are computed by using a first-order finite difference scheme and the radial basis functions. The system of nonlinear PDEs is solved iteratively, and the nonlinear terms are treated by using the DRBEM coordinate matrix. The grid independence test is carried out, and it is found that $N = 336$ gives grid independent solutions for $Mn = 10$ and $I_r = 1$ case. The number of boundary nodes needs to be increased according to the magnetic number due to the alternations in the flow and pressure profiles. The influences of the magnetic field strength and the current intensity ratios are researched for moderate values of Mn. It is found that the velocity and the pressure profiles are dominated by the strong point magnetic source. An increment in the magnetic field strength results in an accelerated flow on the transverse plane, retardation in the axial flow, and an increase in the pressure, especially in front of the strong point magnetic source. When the strength of one of the sources increases further, the flow behaves as if it was under the influence of a single point magnetic source, and the pressure around the weak source decreases. The proposed numerical scheme is capable of catching flow fluctuations, and the boundary discretization nature of DRBEM provide solutions with a less computational cost. In the present study, the FHD flow is investigated in an irregular cavity with smooth boundary sections. In the subsequent works, it is worthy to research the effects of the unsmooth boundary [13,18,43] and analyze the hydrodynamic instability of the present FHD flow [5,8,12].

Declaration of Competing Interests The author declares that there is no competing interests.

Acknowledgements The author thanks to the reviewers for their valuable suggestions.

References

[1] Akter, S., Ferdows, M., Shamshuddin, M.D., Siri, Z., Similarity solution for induced magnetic field boundary layer flow of metallic nanofluids via convectively inclined stationary/moving flat plate:Spectral relaxation computation, *Journal of Applied Mathematics and Mechanics, 102* (2022), e202100179, https://dx.doi.org/10.1002/zamm.202100179.

[2] AL-Bayati, S.A., Wrobel, L.C., A novel dual reciprocity boundary element formulation for two-dimensional transient convection-diffusion-reaction problems with variable velocity, *Engineering Analysis with Boundary Elements, 94* (2018), 60–68, https://dx.doi.org/10.1016/j.enganabound.2018.06.001.

[3] Al-Kouz, W., Abderrahmane, A., Shamshuddin, M.D., Younis, O., Mohammed, S., Beg, O.A., Toghraie, D., Heat transfer and entropy generation analysis of water-Fe_3O_4/CNT hybrid magnetic nanofluid flow in a trapezoidal wavy enclosure containing porous media with Galerkin finite element method, *The European Physical Journal Plus, 136* (2021), 1184, https://dx.doi.org/10.1140/epjp/s13360-021-02192-3.

[4] Brebbia, C.A., Dominguez, J., Boundary Elements and Introductory Course, WIT Press/Computational Mechanics Publications, 1992.

[5] Curtis, R.A., Flows and wave propagation in ferrofluids, *The Physics of Fluids, 14(10)* (1971), 2096–2101, https://dx.doi.org/10.1063/1.1693299.

[6] Dalvi, S., Meer, T.H., Shahi, M., Numerical evaluation of the ferrofluid behavior under the influence of three-dimensional non-uniform magnetic field, *International Journal of Heat and Fluid Flow, 94* (2022), 108901, https://dx.doi.org/10.1016/j.ijheatfluidflow.2021.108901.

[7] Fattah, A.R.A., Ghosh, S., Puri, I.K., Printing microstructures in a polymer matrix using a ferrofluid droplet, *Journal of Magnetism and Magnetic Materials, 401* (2016), 1054–1059, https://dx.doi.org/10.1016/j.jmmm.2015.10.112.

[8] Finlayson, B.A., Convective instability of ferromagnetic fluids, *Journal of Fluid Mechanics, 40(4)* (1970), 753–767, https://dx.doi.org/10.1017/S0022112070000423.

[9] Fletcher, C.A.J., Computational Techniques for Fluid Dynamics 2, Springer, Berlin, 1991.

[10] Goharkhah, M., Ashjaee, M., Effect of an alternating nonuniform magnetic field on ferrofluid flow and heat transfer in a channel, *Journal of Magnetism and Magnetic Materials, 362* (2014), 80–89, https://dx.doi.org/10.1016/j.jmmm.2014.03.025.

[11] Han Aydin, S., Tezer-Sezgin, M., A DRBEM solution for MHD pipe flow in a conducting medium, *Journal of Computational and Applied Mathematics, 259(B)* (2014), 720–729, https://dx.doi.org/10.1016/j.cam.2013.05.010.

[12] He, J.H., Moatimid, G.M., Sayed, A., Nonlinear EHD instability of two-superposed Walters' B fluids through porous media, *Axioms, 10* (2021), 258, https://dx.doi.org/10.3390/axioms10040258.

[13] He, J.H., Qie, N., He, C.H., Solitary waves travelling along an unsmooth boundary, *Results in Physics, 24* (2021), 104104, https://dx.doi.org/10.1016/j.rinp.2021.104104.

[14] Huang, X., Zhang, X., Wang, Y., Numerical simulation of ferrofluid-lubricated rough elliptical contact with start-up motion, *Applied Mathematical Modelling, 91* (2021), 232–260, https://dx.doi.org/10.1016/j.apm.2020.09.004.

[15] Humane, P.P., Patil, V.S., Patil, A.B., Shamshuddin, M.D., Rajput, G.R., Dynamics of multiple slip boundaries effect on MHD Casson-Williamson double-diffusive nanofluid flow past an inclined magnetic stretching sheet, In *Proceedings of the Institution of Mechanical Engineers, Part E: Journal of Process Mechanical Engineering* (2022), vol. 236(5), pp. 1906–1926, https://dx.doi.org/10.1177/09544089221078153.

[16] Javaran, S.H., Khaji, N., Dynamic analysis of plane elasticity with new complex Fourier radial basis functions in the dual reciprocity boundary element method, *Applied Mathematical Modelling, 38(14)* (2014), 3641–3651, https://dx.doi.org/10.1016/j.apm.2013.12.010.

[17] Kenjeres, S., Numerical analysis of blood flow in realistic arteries subjected to strong non-uniform magnetic fields, *International Journal for Heat and Fluid Flow, 29* (2008), 752–764, https://dx.doi.org/10.1016/j.ijheatfluidflow.2008.02.014.

[18] Li, X., Wang, D., Effects of a cavity's fractal boundary on the free front interface of the polymer filling stage, *Fractals, 29(7)* (2021), 2150225, https://dx.doi.org/10.1142/S0218348X2150225X.

[19] Loukopoulos, V.C., Tzirtzilakis, E.E., Biomagnetic channel flow in spatially varying magnetic field, *International Journal of Engineering Science, 42* (2004), 571–590, https://dx.doi.org/10.1016/j.ijengsci.2003.07.007.

[20] Micchelli, C.A., Interpolation of scattered data:Distance matrices and conditionally positive definite functions, *Constructive approximation, 2* (1986), 11–22, https://dx.doi.org/10.1007/BF01893414.

[21] Mortazavinejad, S.M., Mozafarifard, M., Numerical investigation of two-dimensional heat transfer of an absorbing plate of a flat-palet solar collector using dual-reciprocity method based on boundary element, *Solar Energy, 191* (2019), 332–340, https://dx.doi.org/10.1016/j.solener.2019.08.075.

[22] Mousavi, S.M., Darzi, A.A.R., Akbari, O.A., Toghraie, D., Marzban, A., Numerical study of biomagnetic fluid flow in a duct with a constriction affected by a magnetic field, *Journal of Magnetism and Magnetic Meterials, 473* (2019), 42–50, https://dx.doi.org/10.1016/j.jmmm.2018.10.043.

[23] Mousavi, S.M., Farhadi, M., Sedighi, K., Effect of non-uniform magnetic field on biomagnetic fluid flow in a 3D channel, *Applied Mathematical Modelling, 40* (2016), 7336–7348, https://dx.doi.org/10.1016/j.apm.2016.03.012.

[24] Partridge, P.W., Brebbia, C.A., Wrobel, L.C., The Dual Reciprocity Boundary Element Method, Computational Mechanics Publications, Sauthampton, Boston, 1992.

[25] Patil, V.S., Shamshuddin, M.D., Ramesh, K., Rajput, G.R., Slipperation of thermal and flow speed impacts on natural convective two-phase nanofluid model across Riga surface: Computational scrutinization, *International Communications in Heat and Mass Transfer, 135* (2022), 106135, https://dx.doi.org/10.1016/j.icheatmasstransfer.2022.106135.

[26] Plansey, R., Collin, R.E., Principles and Applications of Electromagnetic Fields, Mc Graw-Hill, NewYork, 1961.

[27] Rosensweig, R.E., Ferrohydrodynamics, Dover Publications, Mineola, New York, 2014.

[28] Salawu, S.O., Obalalu, A.M., Shamshuddin, M.D., Nonlinear solar thermal radiation efficiency and energy optimization for magnetized hybrid Prandtl-Erying nanoliquid in aircraft, *Arabian Journal for Science and Engineering* (2022), https://dx.doi.org/10.1007/s13369-022-07080-1.

[29] Salehpour, A., Ashjaee, M., Effect of different frequency functions on ferrofluid FHD flow, *Journal of Magnetism and Magnetic Materials, 480* (2019), 112–131, https://dx.doi.org/10.1016/j.jmmm.2019.02.045.

[30] Senel, P., Flow in a cavity subjected to two variable magnetic sources, In *Abstract book of the Second International Conference on Applied Mathematics in Engineering (ICAME'21)* (Balikesir, Turkey, September 1-3, 2021), p. 73.

[31] Senel, P., Tezer-Sezgin, M., DRBEM solution to MHD flow in ducts with thin slipping side walls and separated by conducting thick Hartmann walls, *Computers and Mathematics with Applications, 78* (2019), 3165–3174, https://dx.doi.org/10.1016/j.camwa.2019.05.019.

[32] Seo, J.H., Lee, M.Y., Illuminance and heat transfer characteristics of high power LED cooling system with heat sink filled with ferrofluid, *Applied Thermal Engineering, 143* (2018), 438–449, https://dx.doi.org/10.1016/j.applthermaleng.2018.07.079.

[33] Shahzad, F., Jamshed, W., Sajid, T., Shamshuddin, M.D., Safdar, R., Salawu, S.O., Eid, M.R., Hafeez, M.B., Krawczuk, M., Electromagnetic control dynamics of generalized Burgers' nanoliquid flow containing motile microorganisms with Cattaneo-Christov relations: Galerkin finite element machanism, *Applied Sciences, 12(17)* (2022), 8636, https://dx.doi.org/10.3390/app12178636.

[34] Shamshuddin, M.D., Ghaffari, A., Usman, Radiative heat energy exploration on Casson-type nanoliquid induced by a convectively heated porous plate in conjuction with thermophoresis and Brownian movements, *International Journal of Ambient Energy, 43(1)* (2022), 6329–6340, https://dx.doi.org/10.1080/01430750.2021.2014960.

[35] Shamshuddin, M.D., Mabood, F., Rajput, G.R., Beg, O.A., Badruddin, I.A., Thermo-solutal dual stratified convective magnetized fluid flow from an exponentially stretching Riga plate sensor surface with thermophoresis, *International Communications in Heat and Mass Transfer, 134* (2022), 105997, https://dx.doi.org/10.1016/j.icheatmasstransfer.2022.105997.

[36] Sharifi, A., Motlagh, S.Y., Badfar, H., Ferro hydro dynamic analysis of heat transfer and biomagnetic fluid flow in channel under the effect of two inclined permanent magnets, *Journal of Magnetism and Magnetic Materials, 472* (2019), 115–122, https://dx.doi.org/10.1016/j.jmmm.2018.10.029.

[37] Sheikholeslami, M., Rashidi, M.M., Effect of space dependent magnetic field on free convection of Fe_3O_4 -water nanofluid, *Journal of the Taiwan Institute of Chemical Engineers, 56* (2015), 6–15, https://dx.doi.org/10.1016/j.jtice.2015.03.035.

[38] Sheikholeslami, M., Rashidi, M.M., Ferrofluid heat transfer treatment in the presence of variable magnetic field, *The European Physical Journal Plus, 130* (2015), 115–126, https://dx.doi.org/10.1140/epjp/i2015-15115-4.

[39] Siddiqa, S., Begum, N., Safdar, S., Hossain, M.A., Al-Rashed, A.A.A.A., Influence of localized magnetic field and strong viscosity on the biomagnetic fluid flow in a rectangular duct, *International Journal of Mechanical Sciences, 131-132* (2017), 451–458, https://dx.doi.org/10.1016/j.ijmecsci.2017.07.022.

[40] Soltanipour, H., Numerical analysis of two-phase ferrofluid forced convection in an annulus subjected to magnetic sources, *Applied Thermal Engineering, 196* (2021), 117278, https://dx.doi.org/10.1016/j.applthermaleng.2021.117278.

[41] Tzirtzilakis, E.E., A mathematical model for blood flow in a magnetic field, *Physics of Fluids, 17:077103* (2005), 1–15, https://dx.doi.org/10.1063/1.1978807.

[42] Tzirtzilakis, E.E., Sakalis, V.D., Kafoussias, N.G., Hatzikonstantinou PM, Biomagnetic fluid flow in a 3D rectangular duct, *International Journal for Numerical Methods in Fluids, 44* (2004), 1279–1298, https://dx.doi.org/10.1002/fld.618.

[43] Wu, P.X., Yang, Q., He, J.H., Solitary waves of the variant Boussinesq-Burgers equation in a fractal-dimensional space, *Fractals, 30(3)* (2022), 2250056, https://dx.doi.org/10.1142/S0218348X22500566.

[44] Wu, V.M., Huynh, E., Tang, S., Uskokovic, V., Brain and bone cancer targeting by a ferrofluid composed of superparamagnetic iron-oxide/silica/carbon nanoparticles (earthicles), *Acta Biomaterialia, 88* (2019), 422–447, https://dx.doi.org/10.1016/j.actbio.2019.01.064.

[45] Yu, B., Cao, G., Huo, W., Zhou, H., Atroshchenko, E., Isogeometric dual reciprocity boundary element method for solving transient heat conduction problems with heat sources, *Journal of Computational and Applied Mathematics, 385* (2021), 113197, https://dx.doi.org/10.1016/j.cam.2020.113197.

[46] Yu, B., Zhou, H.L., Chen, H.L., Tong, Y., Precise time-domain expanding dual reciprocity boundary element method for solving transient heat conduction problems, *International Journal of Heat and Mass Transfer, 91* (2015), 110–118, https://dx.doi.org/10.1016/j.ijheatmasstransfer.2015.07.109.

[47] Zeng, J., Deng, Y., Vedantam, P., Tzeng, T.R., Xuan, X., Magnetic separation of particles and cells in ferrofluid flow through a straight microchannel using two offset magnets, *Journal of Magnetism and Magnetic Materials, 346* (2013), 118–123, https://dx.doi.org/10.1016/j.jmmm.2013.07.021.

[48] Zhang, T., Wen, Z., Lei, H., Gao, Z., Chen, Y., Zhang, Y., Liu, J., Xie, Y., Sun, X., Surface-microengineering for high-performance triboelectric tactile sensor via dynamically assembled ferrofluid template, *Nano Energy, 87* (2021), 106215, https://dx.doi.org/10.1016/j.nanoen.2021.106215.